

2015 IEEE Applied Power Electronics Conference, March 2015

# Impedance Control Network Resonant dc-dc Converter for Wide-Range High-Efficiency Operation

Jie Lu\*, David J. Perreault\*\* and Khurram K. Afridi\*

\*Department of Electrical, Computer, and Energy Engineering  
University of Colorado Boulder  
Boulder, CO 80309, USA  
jie.lu@colorado.edu; khurram.afridi@colorado.edu

\*\*Department of Electrical Engineering and Computer Science  
Massachusetts Institute of Technology  
Cambridge, MA 02139, USA  
djperrea@mit.edu

**Abstract**—This paper introduces a new resonant converter architecture that utilizes multiple inverters and a lossless impedance control network (ICN) to maintain zero voltage switching (ZVS) and near zero current switching (ZCS) across wide operating ranges. Hence, the ICN converter is able to operate at fixed frequency and maintain high efficiency across wide ranges in input and output voltages and output power. The ICN converter architecture enables increase in switching frequency (hence reducing size and mass) while achieving very high efficiency. A prototype 200 W, 500 kHz ICN resonant converter designed to operate over an input voltage range of 25 V to 40 V and output voltage range of 250 V to 400 V is built and tested. The prototype ICN converter achieves a peak efficiency of 97.2%, maintains greater than 96.2% full power efficiency at 250 V output voltage across the nearly 2:1 input voltage range, and maintains full power efficiency above 94.6% across its full input and output voltage range. It also maintains efficiency above 93.4% over a 10:1 output power range across its full input and output voltage range owing to the use of burst-mode control.

**Keywords**—dc/dc converter; resonant converter; high-efficiency converter; converter for wide-range operation; impedance control network; on/off control; burst mode.

## I. INTRODUCTION

Compact isolated converters operating at large conversion ratios are needed for applications ranging from off-line power supplies for electronic loads to solar micro-inverters. Such converters based on conventional architectures often do not achieve very high efficiencies, and their efficiencies typically drop from peak values as the operating conditions change. To achieve the highest efficiencies, high power density converters must operate using soft-switching techniques – zero voltage switching (ZVS) and/or zero current switching (ZCS) – to limit transistor switching losses. Unfortunately, while conventional soft-switching converter architectures can achieve soft-switching under specific operating conditions, it is difficult to maintain desirable circuit waveforms (e.g., ZVS/ZCS switching and minimum conduction current) as power is reduced from maximum and as the input voltage varies from nominal.

To understand this challenge, consider some widely-used design and control techniques. One common means of controlling resonant soft-switched converters is frequency

control, in which the output voltage is regulated in the face of load and input voltage variations by modulating the converter switching frequency [1], [2]. Because of the inductive loading requirements to achieve ZVS switching, power is reduced in such converters by increasing switching frequency, exacerbating switching loss. Wide frequency operation also makes design of magnetic components and EMI filters more challenging. Moreover, depending on resonant tank design, circulating currents in the converter may not back off with power, reducing efficiency. An alternative method is phase-shift control [3], [4] or “outphasing” control, in which the relative timing of multiple inverter legs are modulated to control power. However, conventional full-bridge resonant converters using phase shift control suffer from asymmetric current levels between the two inverter legs at the switching instants as the legs are outphased to reduce output power, as shown in Fig. 1. The result is that the transistors in the leading

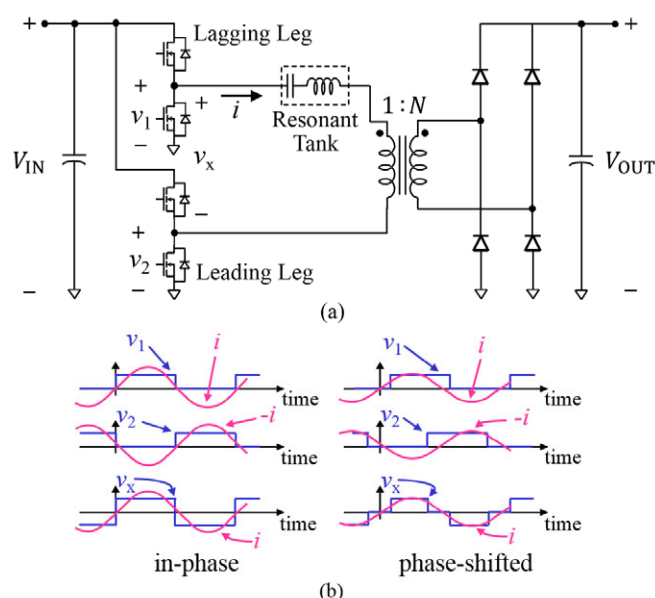


Fig. 1. Asymmetric current levels at switching instants between two inverter legs and eventual loss of ZVS in (a) conventional full-bridge series resonant dc-dc converter as (b) the two inverter legs are phase-shifted to control output voltage or power.

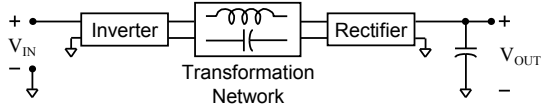


Fig. 2. Block diagram for a conventional dc-dc resonant converter.

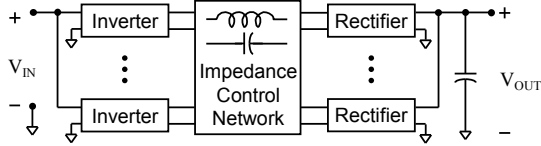


Fig. 3. Architecture of the proposed impedance control network (ICN) resonant converter. Note that while an input parallel connection of inverter inputs is shown, a series connection voltage may also be employed, and can be advantageous for voltage step-down designs.

inverter leg start to turn-off at large currents. Also, as outphasing is increased further the transistors in the lagging inverter leg lose ZVS turn-on capability. These factors result in extra losses and lead to lower converter efficiency at partial loads, and consequently to poor design tradeoffs. Other fixed frequency control techniques have also been developed [5], [6]. However, these also lose zero voltage switching (ZVS) capability as the output power is reduced [7]. Hence, there is need for circuit designs and associated controls that can provide reduced loss when operating over wide input voltage and power ranges, and can provide large voltage conversion ratios.

This paper introduces a new resonant converter architecture that operates at fixed frequency and utilizes a lossless impedance control network (ICN) to maintain ZVS and near-ZCS across wide operating ranges in terms of input/output voltages and output power, minimizing device stress and switching loss, and enabling both high efficiency and power density. A prototype 200 W, 500 kHz ICN resonant converter designed to operate over an input voltage range of 25 V to 40 V and output voltage range of 250 V to 400 V is built and tested. The prototype ICN converter achieves a peak efficiency of 97.2%, maintains greater than 96.2% full power efficiency at 250 V output voltage across the nearly 2:1 input voltage range, and maintains full power efficiency above 94.6% across its full input and output voltage range. It also maintains efficiency above 93.4% over a 10:1 output power range across its full input and output voltage range owing to the use of burst-mode control.

## II. IMPEDANCE CONTROL NETWORK (ICN) RESONANT CONVERTER

Resonant dc-dc converters comprise an inverter stage, a transformation stage, and a rectifier stage, as shown in Fig. 2. Figure 3 shows the architecture of the proposed impedance control network (ICN) resonant dc-dc converter. It incorporates multiple inverters and one or more rectifiers operated together under phase-shift control, along with a transformation stage incorporating an impedance control network (ICN). The ICN draws upon the concepts of lossless power combiners and resistance compression networks [8]-[13]. The ICN provides a

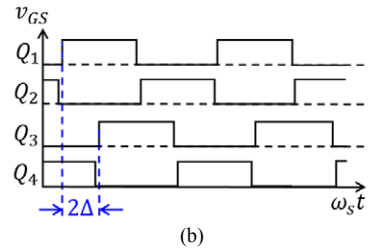
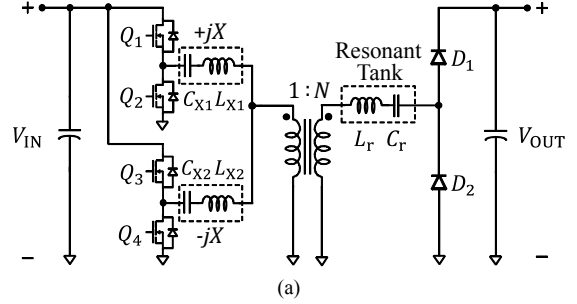


Fig. 4. One implementation of an impedance control network (ICN) resonant converter, appropriate for voltage step-up: (a) converter topology and (b) switch gating signals.

differential phase shift in the voltages and currents whereby the effective impedances seen at its inputs look highly resistive at the fundamental frequency, enabling switching of the inverters at zero current across wide operating ranges<sup>1</sup>. By modifying the networks for slightly inductive loading of the inverters, one can realize simultaneous zero-voltage and near-zero-current switching.

There are many possible implementations of the ICN converter. A specific implementation suitable for widely varying input voltages is shown in Fig. 4. The converter is operated at a fixed switching frequency and each inverter is operated at a fixed duty ratio (~50%). When the switching frequency of the converter matches the resonant frequency of the resonant tank, and the two branches of the impedance control network are designed to have equal but opposite reactances ( $+jX$  and  $-jX$ ) at the switching frequency, the effective admittances seen by the two inverters ( $Y_1$  and  $Y_2$ ) under fundamental frequency approximation are given by:

$$Y_1 = Y_2^* = \frac{V_{OUT} \sin \Delta}{NV_{IN} X} + j \left( \frac{V_{OUT} \cos \Delta}{NV_{IN} X} - \frac{1}{X} \right). \quad (1)$$

Here  $V_{IN}$  is the input voltage,  $V_{OUT}$  is the output voltage,  $N$  is the transformer turns ratio, and  $2\Delta$  is the phase shift between the two inverters. With this design, the effective susceptance seen by the two inverters can be made zero or arbitrarily small when the two inverters are operated with a specific phase shift between them, as illustrated in Fig. 5. The phase shift at which the susceptance seen by the inverters becomes zero is a function of the input-output voltage ratio and given by:

$$2\Delta = 2 \cos^{-1} \left( \frac{NV_{IN}}{V_{OUT}} \right). \quad (2)$$

Hence, by varying this phase shift as the input or output voltage

<sup>1</sup> Here “effective impedance” means the voltage-to-current (V/I) ratio observed at a port with all sources and loads active.

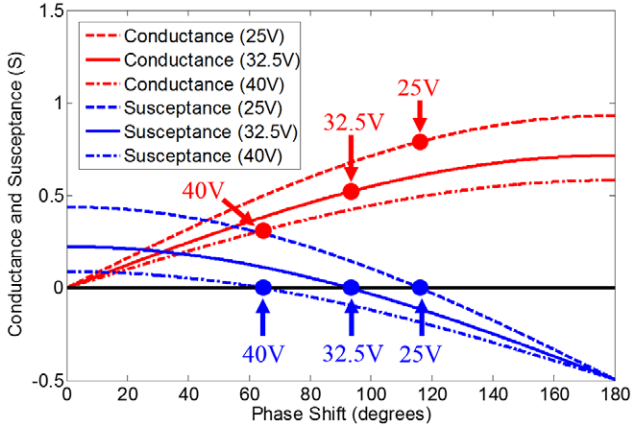


Fig. 5. Effective conductance and susceptance seen by the two inverters as a function of their relative phase shift for three input voltage values: 25 V, 32.5 V and 40 V. Output voltage is 250 V in all cases.

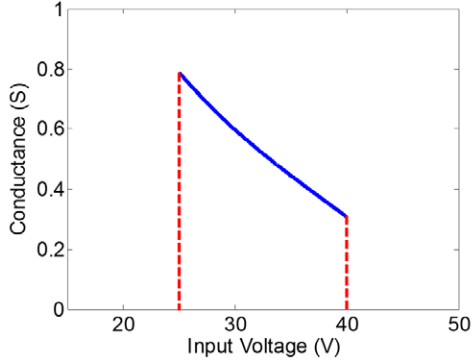


Fig. 6. Effective conductance seen by two inverters as a function of input voltage when ICN converter is operated with zero effective susceptance, at output voltage of 250V.

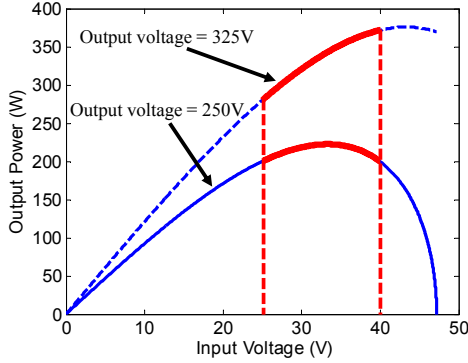


Fig. 7. Variation in output power as a function of input voltage for the ICN converter operated with the phase-shift between the two inverters controlled to provide zero effective susceptance seen by the inverters.

varies, the admittance seen by the inverters can be kept purely conductive across the full input and output voltage operating range of the dc-dc converter. By operating the converter at a switching frequency slightly higher than the resonant frequency of the  $L_r$ - $C_r$  tank, both the inverters can be slightly inductively loaded to achieve ZVS. This allows the inverter switches to have simultaneous zero-voltage switching and near zero-current switching capability, thus minimizing switching losses

and reactive currents, boosting converter efficiency over wide input and output voltage ranges.

At a given switching frequency, the output power of an inverter is proportional to the square of the input voltage and the conductance seen by the inverter. In conventional designs, this can often lead to large variations in power delivery with input voltage that must be addressed (e.g., through oversizing of the inverter components and use of frequency control to modulate power). However, since the effective conductance seen by the inverters in the ICN converter (operated at near zero effective susceptance) decreases with input voltage (see Fig. 5 and Fig. 6), the variation in output power with input voltage can be made quite limited across a wide input voltage range, as shown in Fig. 7, and expressed mathematically as:

$$P_{\text{OUT}} = \frac{4V_{\text{IN}}\sqrt{V_{\text{OUT}}^2 - N^2V_{\text{IN}}^2}}{\pi^2NX}. \quad (3)$$

This enables improved sizing of inverter components and use of fixed-frequency operation, with consequent benefits for efficiency. Output power of the converter can be further controlled (for values below that indicated in Fig. 7) using burst mode (on/off) control, in which the operation of the converter is modulated on and off at a frequency much lower than its switching frequency [14], [15]. On/off control is desirable because converter losses back off proportionally to power delivered, thus enabling efficient operation to be maintained over a wide power range. Thus, with the proposed architecture we are able to achieve wide voltage and power range operation at fixed switching frequency and high efficiency.

### III. PROTOTYPE DESIGN

The ICN resonant converter - shown in Fig. 4 - has been designed and built with specifications suitable as an interface between a solar photovoltaic (PV) module and a dc distribution system: an input voltage range of 25 V to 40 V, an output voltage range of 250 V to 400 V, and a maximum output power of 200 W. The converter is designed for a switching frequency of 500 kHz. The output power of the ICN converter increases with output voltage (see Fig. 7); therefore, if maximum output power can be delivered at minimum output voltage then maximum output power can be delivered at all output voltages. Also given the variation in output power with input voltage (see Fig. 7), the need for burst mode control can be minimized if the converter is designed to deliver the same output power at its minimum and maximum input voltages,  $V_{\text{IN,min}}$  and  $V_{\text{IN,max}}$ , respectively. This requirement can be met at the minimum output voltage  $V_{\text{OUT,min}}$  if the transformer turns ratio  $N$  and the reactance  $X$  of the impedance control network are selected using:

$$N = \frac{V_{\text{OUT,min}}}{\sqrt{V_{\text{IN,min}}^2 + V_{\text{IN,max}}^2}}, \quad (4)$$

$$X = \frac{4V_{\text{IN,min}}\sqrt{V_{\text{OUT,min}}^2 - N^2V_{\text{IN,min}}^2}}{\pi^2NP_{\text{OUT,max}}}. \quad (5)$$

For the given design specifications,  $N$  is 5.3 and  $X$  is 2.03  $\Omega$ .

Once the required differential reactance  $X$  is known, the values of the individual reactive components can be determined

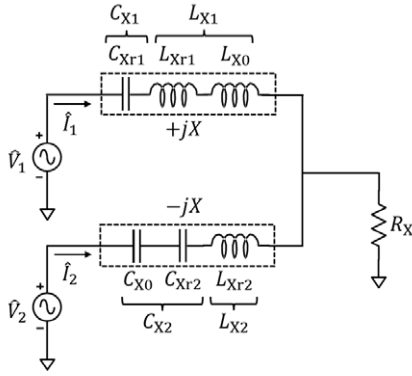


Fig. 8. Primary side reactive elements broken up into their conceptual constituents: differential reactances  $L_{X0}$  and  $C_{X0}$ , and series resonant tank elements ( $L_{Xr1}$ ,  $C_{Xr1}$ ,  $L_{Xr2}$  and  $C_{Xr2}$ ). In the top branch,  $L_{X0}$  and  $L_{Xr1}$  collectively form  $L_{X1}$  and  $C_{Xr1}$  is simply  $C_{X1}$  of Fig. 4. In the bottom branch,  $C_{X0}$  and  $C_{Xr2}$  collectively form  $C_{X2}$  and  $L_{Xr2}$  is simply  $L_{X2}$  of Fig. 4. The  $\hat{V}_1$  and  $\hat{V}_2$  are the fundamental components of the output voltages of the inverters, and the  $\hat{I}_1$  and  $\hat{I}_2$  are the fundamental components of the output currents of the inverters.

by selecting appropriate quality factors for the resonant networks to obtain adequate filtering of the higher-order harmonics. To determine these reactive component values it is simplest to first split  $L_{X1}$  of Fig. 4 into two series inductors  $L_{X0}$  and  $L_{Xr1}$ ; and split  $C_{X2}$  into two series capacitors  $C_{X0}$  and  $C_{Xr2}$ , as shown in Fig. 8. Also  $C_{X1}$  is relabelled as  $C_{Xr1}$  and  $L_{X2}$  is relabelled as  $L_{Xr2}$ . Hence, both branches of the impedance control network contain series resonant tanks (comprising  $L_{Xr1}$ ,  $C_{Xr1}$ ,  $L_{Xr2}$  and  $C_{Xr2}$ ) that are tuned to a resonant frequency slightly below the switching frequency to filter out the higher order harmonics of the switching frequency and achieve ZVS. The elements  $L_{X0}$  and  $C_{X0}$  provide the necessary differential reactance in top and bottom branch, respectively. The values of these differential reactive elements are determined using:

$$L_{X0} = \frac{X}{\omega_s}, \quad (6)$$

$$C_{X0} = \frac{1}{X\omega_s}, \quad (7)$$

where  $\omega_s$  is the angular switching frequency of the converter. The values of the resonant tank elements are determined using:

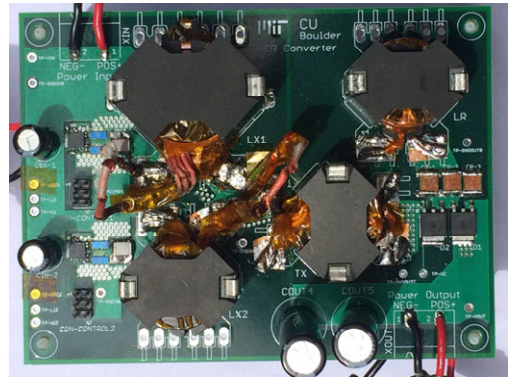
$$L_{Xr1} = \frac{Z_{0X1}}{\omega_s}, \quad L_{Xr2} = \frac{Z_{0X2}}{\omega_s}, \quad (8)$$

$$C_{Xr1} = \frac{1}{Z_{0X1}\omega_s}, \quad C_{Xr2} = \frac{1}{Z_{0X2}\omega_s}, \quad (9)$$

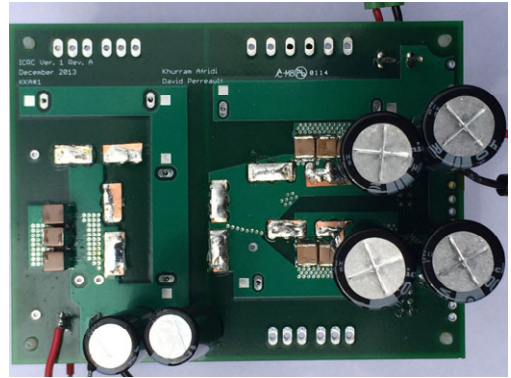
where  $Z_{0X1}$  and  $Z_{0X2}$  are the desired characteristic impedances of the tanks ( $\equiv \sqrt{L_{Xr1}/C_{Xr1}}$  and  $\sqrt{L_{Xr2}/C_{Xr2}}$ , respectively). Their values are determined from  $Z_{0X1} = Q_{0X1}R_X$  and  $Z_{0X2} = Q_{0X2}R_X$ , where  $Q_{0X1}$  and  $Q_{0X2}$  are the desired loaded quality factors of the resonant tanks, and  $R_X (= 2V_{OUT}^2/\pi^2N^2P_{OUT})$  is the equivalent resistance of the rectifier referred to the primary side of the transformer. To achieve reasonable filtering while limiting magnetic losses to acceptable levels in our example, the quality factors  $Q_{0X1}$  and  $Q_{0X2}$  are chosen to be approximately one ( $Q_{0X1} = 0.96$  and  $Q_{0X2} = 1.13$ ) when  $R_X$  has

TABLE I  
Components Used in the Prototype ICN Resonant Converter

Component	Designed Value	Actual Value	Description
$Q_1, Q_2,$ $Q_3, Q_4$	-	-	EPC2001 100-V/25-A eGaN FETs
$D_1, D_2$	-	-	C3D02060E Schottky 600-V/2-A
$L_{X1}$	1.33 $\mu\text{H}$	1.38 $\mu\text{H}$	RM12 EPCOS N49 (4 turns 6000/48AWG)
$C_{X1}$	147 nF	141 nF	250-V NP0
$L_{X2}$	0.81 $\mu\text{H}$	0.84 $\mu\text{H}$	RM10 EPCOS N49 (3 turns 4000/48AWG)
$C_{X2}$	69.6 nF	68 nF	250-V NP0
$L_r$	19.1 $\mu\text{H}$	18.8 $\mu\text{H}$	RM10 EPCOS N49 (19 turns 450/46AWG)
$C_r$	4.9 nF	4.66 nF	1000-V Mica
$T_x$	1 : 5.3	1 : 5.33	RM10 EPCOS N49 Primary 3 turns 2000/48AWG Secondary 16 turns 450/46AWG Leakage inductance referred to the secondary side: 2.16 $\mu\text{H}$
$C_{IN}$	2.2 mF $\times$ 4	2.2 mF $\times$ 4	63-V electrolytic capacitors
$C_{OUT}$	47 $\mu\text{F}$ $\times$ 4	47 $\mu\text{F}$ $\times$ 4	450-V electrolytic capacitors



(a)



(b)

Fig. 9. Photograph of the (a) top and (b) bottom of the prototype ICN resonant converter.

its minimum value of 2.25  $\Omega$  (corresponding to the operating point  $V_{OUT} = 250$  V and  $P_{OUT} = 200$  W). For the given specifications, the values of the primary side reactive components are:  $L_{X1} = L_{X0} + L_{Xr1} = 0.645$   $\mu\text{H} + 0.685$   $\mu\text{H} = 1.33$   $\mu\text{H}$ ,  $C_{X1} = C_{Xr1} = 147$  nF,  $L_{X2} = L_{Xr2} = 0.81$   $\mu\text{H}$ , and  $C_{X2} = C_{Xr2} \parallel C_{X0} = 125$  nF  $\parallel$  157.1 nF = 69.6 nF. The values of the series

resonant tank components ( $L_r$  and  $C_r$ ) on the secondary side of the transformer (in Fig. 4) are selected in a similar fashion. Again a quality factor of one is used to achieve reasonable filtering while limiting losses. The selected values of these tank elements are:  $L_r = 19.1 \mu\text{H}$  and  $C_r = 4.9 \text{ nF}$ .

The actual components used in fabrication of the prototype ICN resonant converter are listed in Table I. The core material

chosen for the magnetic elements (inductors and transformer) is N49 from EPCOS since it has low losses around 500 kHz. Litz wire is used to wind the inductors and the transformer. The primary side resonant capacitors are 250-V NP0 low-ESR capacitors, while 1-kV mica low-ESR capacitors are used for the secondary side resonant capacitors. For the half-bridge inverters, EPC 100-V/25-A enhancement-mode gallium nitride (GaN) transistors (EPC2001) are used. These are driven by half-bridge drivers designed for enhancement-mode GaN transistors (LM5113). For the rectifier stage 600-V/2-A silicon carbide (SiC) Schottky diodes (C3D02060E) are used. The converter is controlled using a Microchip dsPIC33FJ64GS610, a 16-bit digital signal controller with high-speed PWM outputs. Figure 9 shows the top and bottom views of the prototype ICN resonant converter.

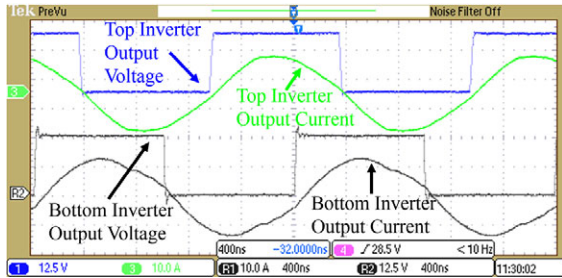
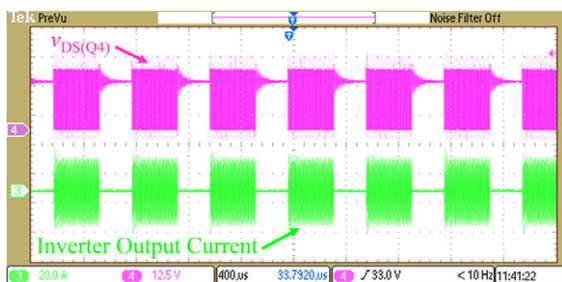
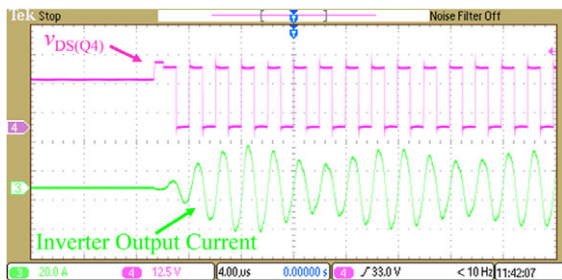


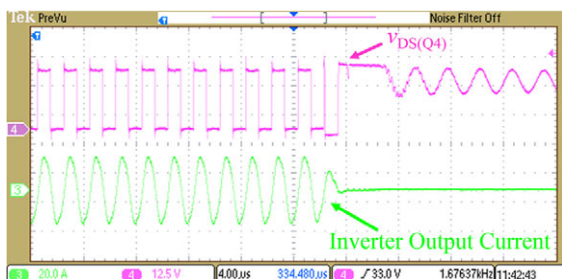
Fig. 10. Measured waveforms for the ICN resonant converter operating at full power (200 W) at 25 V input voltage and 250 V output voltage. Waveforms shown are the output voltage and output current of both (top and bottom) half-bridge inverters.



(a)



(b)



(c)

Fig. 11. Burst mode operation of the ICN resonant converter delivering full power (200 W) at 25 V input voltage and 400 V output voltage. Waveforms shown are the output voltage and output current of the bottom half-bridge inverter: (a) long timescale showing multiple startup and shutdown sequences, (b) zoomed timescale to show the startup dynamics, and (c) zoomed timescale to show the shutdown dynamics.

#### IV. EXPERIMENTAL RESULTS

The 200 W prototype ICN converter has been built and tested. The converter is operated at a switching frequency of 505 kHz, slightly higher than the designed switching frequency, to make the two inverters sufficiently inductively-loaded to achieve zero voltage switching (ZVS). Figure 10 shows the measured waveforms of this converter when operated at full power (200 W) at its minimum input voltage ( $V_{IN} = 25 \text{ V}$ ) and minimum output voltage ( $V_{OUT} = 250 \text{ V}$ ). To deliver full power at these voltages, burst mode (on/off) control is not needed, as the converter produces 200 W of output power when it is running continuously.

Clearly the switches of both the top and the bottom inverters achieve ZVS - and near ZCS. ZVS is achieved as the inverter output current is sufficiently negative during the low to high inverter output voltage transition and sufficiently positive during the high to low inverter output voltage transition. Near ZCS is achieved as the currents are fairly sinusoidal due to the presence of the series resonant tanks with a reasonable loaded quality factor. A useful measure of near ZCS operation is the ratio of the switch current at turn-off to its peak current. The turn-off current for the top inverter is about 2 A, which is about 16% of the peak current value. The turn-off current of the bottom inverter is about 3.2 A, which is about 25% of the peak value of the current.

The waveforms of Fig. 10 can also be used to compare the theoretically-required phase shift between the two inverters and that needed in practice to achieve ZVS and near ZCS operation. In Fig. 10 the phase shift between the two inverters is about 634 ns, which is 32% of the switching period (1.982  $\mu\text{s}$ ) and corresponds to an angle of  $115.16^\circ$ . This is within 0.5% of the theoretically predicted phase shift value ( $115.58^\circ$ ) calculated using (2).

When the output voltage and - to a lesser extent - the input voltage of the converter increase above their minimum values, burst mode control is needed to limit output power to 200 W (see Fig. 7). Burst mode control is also needed at all input/output voltage combinations when the output power is reduced below 200 W. Figure 11 shows the operation of the ICN resonant converter under burst mode control with an input voltage of 25 V, an output voltage of 400 V and the output

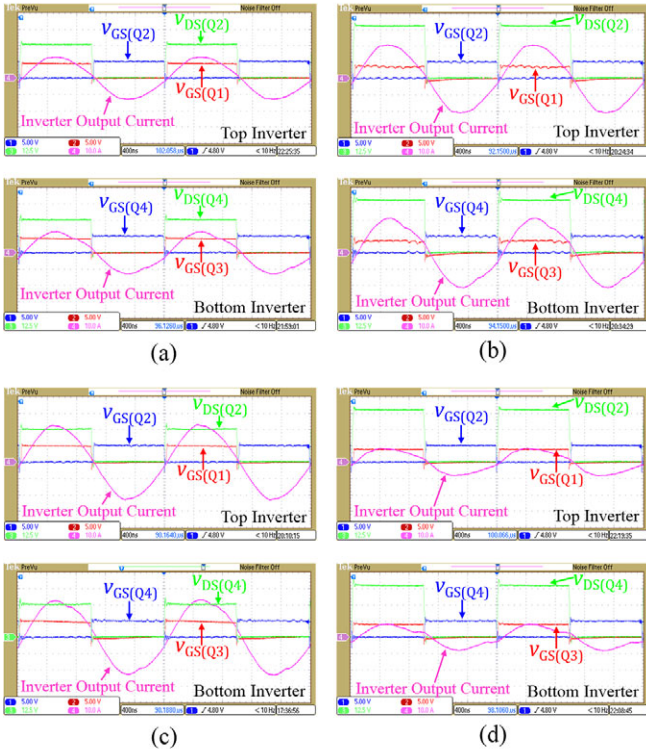


Fig. 12. Measured waveforms confirming ZVS and near ZCS operation of the ICN resonant converter at four extreme operating points in terms of input voltage ( $V_{IN}$ ) and output voltage ( $V_{OUT}$ ): (a)  $V_{IN} = 25$  V,  $V_{OUT} = 250$  V, (b)  $V_{IN} = 40$  V,  $V_{OUT} = 400$  V, (c)  $V_{IN} = 25$  V,  $V_{OUT} = 400$  V, (d)  $V_{IN} = 40$  V,  $V_{OUT} = 250$  V.

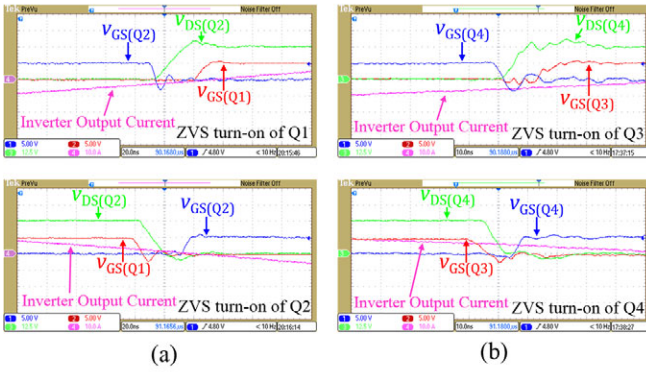


Fig. 13. Measured waveforms confirming ZVS operation of the ICN resonant converter with  $V_{IN} = 25$  V,  $V_{OUT} = 400$  V: (a) ZVS turn-on of the transistors in the top inverter and (b) ZVS turn-on of the transistors in the bottom inverter.

power regulated to 200 W. The burst mode on/off modulation frequency is 1.68 kHz. This value is selected as it provides a good balance between the additional losses in the input capacitors due to the on/off modulation frequency ripple current and the additional losses in the converter due to its repeated startup and shutdown. Figure 11 also shows zoomed-in views of the bottom inverter's output voltage and output current waveforms during converter startup and shutdown.

To validate that the ICN resonant converter achieves ZVS and near ZCS operation across its entire design range, its operation is tested across the specified input voltage, output

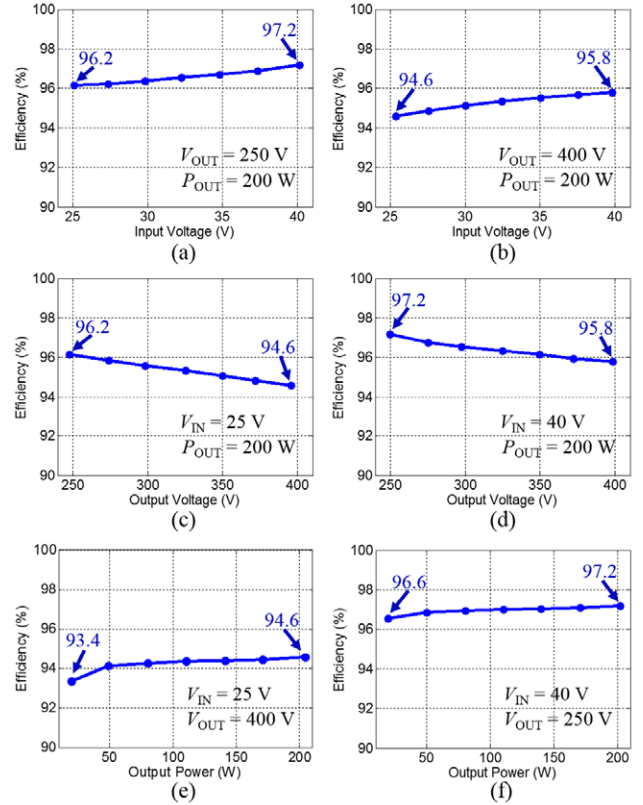


Fig. 14. Measured efficiency of the ICN resonant converter across variations in input voltage ( $V_{IN}$ ), output voltage ( $V_{OUT}$ ) and output power ( $P_{OUT}$ ): (a) variation in input voltage with  $V_{OUT} = 250$  V and  $P_{OUT} = 200$  W, (b) variation in input voltage with  $V_{OUT} = 400$  V and  $P_{OUT} = 200$  W, (c) variation in output voltage with  $V_{IN} = 25$  V and  $P_{OUT} = 200$  W, (d) variation in output voltage with  $V_{IN} = 40$  V and  $P_{OUT} = 200$  W, (e) variation in output power with  $V_{IN} = 25$  V and  $V_{OUT} = 400$  V, and (f) variation in output power with  $V_{IN} = 40$  V and  $V_{OUT} = 250$  V.

voltage and output power ranges. Figure 12 shows the pertinent waveforms of the converter at four extreme operating points as input voltage is varied from 25 V to 40 V and output voltage is varied from 250 V to 400 V, while keeping output power constant at 200 W. Again it is easy to see that both (top and bottom) inverters of the ICN converter achieve ZVS turn-on and near ZCS turn-off at all four operating points. Figure 13 shows the zoomed in view of the switch voltages and currents during the switching transitions when operating with 25 V input and 400 V output. The ZVS turn-on of all the transistors can be observed in Fig. 13. It has been confirmed that the ICN converter achieves ZVS and near ZCS operation across its entire operating range.

The efficiency of the prototype ICN resonant converter has also been measured across its entire operating range. The measured efficiency is displayed in Fig. 14 for various conditions. All the efficiency plots are fairly flat. Figure 14(a) and (b) plot the efficiency of the ICN converter as its input voltage is varied from 25 V to 40 V, while the output voltage and output power are held constant. In both cases output power is 200 W, while output voltage is 250 V in Fig. 14(a) and 400 V in Fig. 14(b). When the output voltage is 250 V, the peak efficiency of the ICN converter is 97.2% and its efficiency does

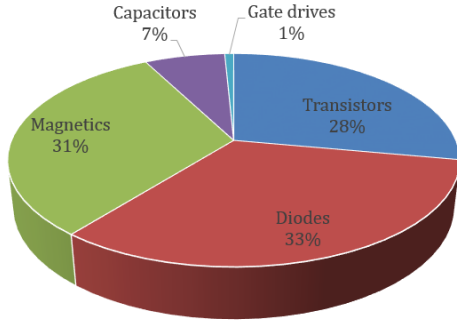


Fig. 15. Loss breakdown of the ICN resonant converter based on theoretical models when the converter is operating at an input voltage of 32.5 V, output voltage of 325 V and output power of 200 W.

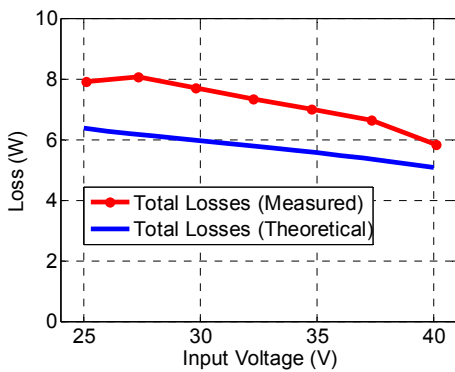


Fig. 16. Comparison of measured and theoretically predicted total losses in the ICN converter as a function of input voltage when the converter is operating at an output voltage of 250 V and output power of 200 W.

not fall below 96.2% as the input voltage is varied across its entire range. The efficiency increases monotonically with increasing input voltage, as primary-side conduction losses are reduced with decreasing input current. The efficiency of the converter reduces at higher output voltages, as the converter has to be operated in burst mode to limit output power. However, at full output power (200 W) the efficiency of the converter never falls below 94.6%, which occurs at the lowest input voltage (25 V) and highest output voltage (400 V).

Figure 14(c) and (d) plot the efficiency of the ICN converter as its output voltage is varied from 250 V to 400 V, while the input voltage and output power are held constant. Again in both cases output power is 200 W, while input voltage is 25 V in Fig. 14(c) and 40 V in Fig. 14(d). When the input voltage is 40 V, the efficiency of the converter stays above 95.8% and achieves a peak value of 97.2% when the output voltage is at its minimum (250 V). Again the worst case efficiency is 94.6%, at minimum input voltage (25 V) and maximum output voltage (400 V).

The efficiency of the ICN converter as the output power is varied is plotted in Fig. 14(e) and (f). In Fig. 14 (e) the input voltage is held at 25 V and the output voltage is held at 400 V and in Fig. 14 (f) the input voltage is held at 40 V and the output voltage is held at 250 V. In both cases burst mode control is

used to vary the output power from 20 W to 200 W. The efficiency of the ICN converter as a function of output power is quite flat, varying by only 0.6% over its entire 10:1 output power range when input voltage is 40 V and output voltage is 250 V. The converter has its lowest efficiency of 93.4% when input voltage is at its minimum (25 V), output voltage is at its maximum (400 V) and output power is at its minimum (20 W). When input voltage is 40 V and output voltage is 250 V the peak efficiency is 97.2% at an output power of 200 W and the efficiency is still above 96.6% at an output power of 20 W. Hence, burst mode control is a good method for regulating output power in an ICN resonant converter.

The efficiency results presented above demonstrate that the ICN resonant converter is able to maintain very high efficiencies across a wide range of operating conditions in terms of input voltage, output voltage and output power. To better understand opportunities for further improvements in efficiency of the ICN converter, a loss breakdown analysis of the converter has been performed based on analytical modeling of the individual loss mechanisms. Figure 15 shows the loss breakdown of the ICN converter when operating at 32.5 V input voltage, 325 V output voltage and 200 W output power. At this operating point, the diode, magnetic and the transistor losses account for the majority of the power losses and they are roughly equal to each other. There are also some losses in the resonant and bypass capacitors. The gate drive losses are very small due to the use of low gate charge GaN transistors. Figure 16 compares the measured and the theoretically predicted total losses in the ICN converter across its full input voltage range when operating at 250 V output voltage and 200 W output power. There is reasonable agreement between the predicted and measured values, and the match is best when input voltage is at its maximum value as PCB trace losses, which are not modeled, are at their minimum.

## V. CONCLUSIONS

This paper presents a new resonant converter architecture that utilizes an impedance control network (ICN) to maintain zero-voltage switching (ZVS) and near zero-current switching (ZCS) across wide operating ranges in terms of input and output voltages and output power. A prototype 200 W, 500 kHz ICN resonant converter designed to operate over an input voltage range of 25 V to 40 V and an output voltage range of 250 V to 400 V is built and tested. It is shown that the converter achieves a peak efficiency of 97.2% and maintains its efficiency above 96.2% for the entire input voltage range when operating at 250 V output voltage and 200 W output power. Furthermore, the converter efficiency stays above 93.4% across its entire input and output voltage ranges and across a 10:1 power range.

## ACKNOWLEDGEMENT

The authors wish to acknowledge the financial support received from the National Science Foundation (NSF) under Award Number 1307699. The authors would also like to thank David Otten of the Massachusetts Institute of Technology (MIT) for providing the control board for this project.

## REFERENCES

- [1] R.L. Steigerwald, "High-Frequency Resonant Transistor DC-DC Converters," *IEEE Transactions on Industrial Electronics*, vol. IE-31, no. 2, pp. 181-191, May 1984.
- [2] R.L. Steigerwald, "A Comparison of Half-Bridge Resonant Converter Topologies," *IEEE Transactions on Power Electronics*, vol. 3, no. 2, pp. 174-182, April 1988.
- [3] J. Vandael and P.D. Ziogas, "A DC to DC PWM Series Resonant Converter Operated at Resonant Frequency," *IEEE Transactions on Industrial Electronics*, vol. 35, no. 3, pp. 451-460, August 1988.
- [4] M.Z. Youssef and P.K. Jain, "A Review and Performance Evaluation of Control Techniques in Resonant Converters," *Proceedings of the IEEE Industrial Electronics Society*, pp. 215-221, Busan, Korea, November, 2004.
- [5] F.S. Tsai, P. Materu and F.C. Lee, "Constant-Frequency Clamped-Mode Resonant Converters," *IEEE Transactions on Power Electronics*, vol. 3, no. 4, pp. 460-473, October, 1988.
- [6] P. Jain, A. St-Martin and G. Edwards, "Asymmetrical Pulse Width Modulated Resonant DC/DC Converter Topologies," *Proceedings of the IEEE Power Electronics Specialists Conference (PESC)*, pp. 818-825, Seattle, WA, June, 1993.
- [7] J.M. Burdío, F. Canales, P.M. Barbosa and F.C. Lee, "A Comparison Study of Fixed-Frequency Control Strategies for ZVS DC/DC Series Resonant Converters," *Proceedings of the IEEE Power Electronics Specialists Conference (PESC)*, pp. 427-432, Vancouver, Canada, June, 2001.
- [8] H. Chireix, "High Power Outphasing Modulation," *Proceedings of the IRE*, vol. 23, no.11, pp. 1370-1392, November 1935.
- [9] Y. Han, O. Leitermann, D.A. Jackson, J.M. Rivas and D.J. Perreault, "Resistance Compression Networks for Radio-Frequency Power Conversion," *IEEE Transactions on Power Electronics*, pp. 41-53, January 2007.
- [10] P.A. Godoy, D.J. Perreault, and J.L. Dawson, "Outphasing Energy Recovery Amplifier with Resistance Compression for Improved Efficiency," *IEEE Transactions on Microwave Theory and Techniques*, vol. 57, no. 12, pp. 2895-2906, December 2009.
- [11] D.J. Perreault, "A New Power Combining and Outphasing Modulation System for High-Efficiency Power Amplification," *IEEE Transactions on Circuits and Systems – I*, vol. 58, no. 8, pp. 1713-1726, August 2011.
- [12] A.S. Jurkov, L. Roslaniec and D.J. Perreault, "Lossless Multi-Way Power Combining and Outphasing for High-Frequency Resonant Inverters," *2012 International Power Electronics and Motion Control Conference*, pp. 910-917, June 2012.
- [13] W. Inam, K.K. Afridi and D.J. Perreault, "High Efficiency Resonant DC/DC Converter Utilizing a Resistance Compression Network," *IEEE Transactions on Power Electronics*, pp. 4126-4135, vol. 29, no. 8, August 2014.
- [14] Y. Lee and Y. Cheng, "A 580 kHz switching regulator using on-off control," *Journal of the Institution of Electronic and Radio Engineers*, vol. 57, no. 5, pp. 221-226, September/October 1987.
- [15] R.C.N. Pilawa-Podgurski, A.D. Sagneri, J.M. Rivas, D.I. Anderson and D.J. Perreault, "High-Frequency Resonant Boost Converters," *IEEE Transactions on Power Electronics*, vol. 24, No. 6, pp. 1654-1665, June 2009.